Energy & Environmental Science

Titanium-oxo clusters reinforced gel polymer electrolyte enabling lithium-sulfur batteries with high gravimetric energy densities

Journal:	*Energy & Environmental Science*
Manuscript ID	EE-ART-09-2020-003005.R1
Article Type:	Paper
Date Submitted by the Author:	16-Dec-2020
Complete List of Authors:	Pei, Fei; Xiamen University Dai, Shuqi ; Xiamen University Guo, Baofu ; Xiamen University Xie, Hao ; Xiamen University Zhao, Chaowei; Jiangxi Academy of Sciences, Research Institute of Applied Chemistry; Xiamen University, Cui, Jingqin; Xiamen University, Fang, Xiaoliang; Xiamen university, Pen-Tung Sah Institute of Micro-Nano Science and Technology Chen, Cheng-Meng; Institute of Coal Chemistry, Chinese Academy of Sciences, Key Laboratory of Carbon Materials; Fritz Haber Institute of the Max Planck Society, Department of Inorganic Chemistry Zheng, Nanfeng; Xiamen University, State Key Laboratory of Physical Chemistry of Solid Surfaces and Department of Chemistry

ARTICLE

Titanium-oxo clusters reinforced gel polymer electrolyte enabling lithium-sulfur batteries with high gravimetric energy densities

Received 00th January 20xx,
Accepted 00th January 20xx

DOI: 10.1039/x0xx00000x

Fei Pei,[a] Shuqi Dai,[a] Baofu Guo,[a] Hao Xie,[a] Chaowei Zhao,[a] Jingqin Cui,[a] Xiaoliang Fang,*[a,b] Chengmeng Chen[c,d] and Nanfeng Zheng*[a,b]

Lithium-sulfur (Li-S) battery research has flourished by upgrading the performances of sulfur cathodes and Li metal anodes under flooded electrolyte conditions. However, since high gravimetric energy density can only be achieved at a low electrolyte/sulfur (E/S) ratio, the severe performance degradation under lean electrolyte conditions is becoming a bottleneck in the development of Li-S batteries. Here we propose a new class of gel polymer electrolytes by using titanium-oxo clusters as reinforcements to construct low E/S batteries. The developed electrolyte has favorable mechanical properties and high Li-ion conductivity, as well as excellent capabilities to block polysulfide shuttling and suppress Li dendrite formation, enabling low E/S batteries to exhibit enhanced capacities and cycling stabilities. Remarkably, the low E/S (3 μL mg_S^{-1}) battery fabricated with high sulfur loading (10 mg_S cm^{-2}) and low negative/positive capacity ratio (1/1) can deliver a gravimetric energy density of 423 Wh kg^{-1} and continue to operate for 100 cycles. This study provides a new avenue for high-energy-density Li-S batteries.

Broader context

Lithium-sulfur (Li-S) batteries are attractive candidates for next-generation rechargeable batteries. Numerous efforts have been made to restrain the shuttling effect of sulfur cathodes and the dendrite growth of Li anodes to increase the capacities and lifespans of Li-S batteries. However, since most of the strategies developed previously are mainly based on high electrolyte/sulfur (E/S) and negative/positive capacity (N/P) ratios, the energy densities of Li-S batteries are far lower than the expectation. How to improve the performance of Li-S batteries under lean electrolyte and limited Li conditions is crucial, but remains challenging. In this work, we successfully utilized titanium-oxo clusters, an important category of organic-inorganic hybrid materials, to fabricate high-performance gel polymer electrolytes for constructing stable and high-energy-density Li-S batteries. With the enhanced mechanical and electrochemical properties, the developed electrolyte enable the low E/S and N/P battery made of commercial carbon materials to deliver a high energy density of 423 Wh kg^{-1}, offering a new strategy for designing advanced Li-S batteries.

Introduction

With the ceiling of energy density approaching, lithium-ion batteries (LIB) are hard to meet the ever-increasing demands for consumer electronics and electric vehicles. In pursuit of energy-dense alternatives to LIB, lithium-sulfur (Li-S) batteries have attracted great attentions due to their high theoretical energy density of 2600 Wh kg^{-1}.[1-3] Tremendous efforts have been devoted to addressing the technical obstacles of Li-S batteries. With regards to sulfur cathodes, the cathode related components including sulfur host,[4-6] binder,[7,8] separator,[9,10] and current collector,[11] have been deeply explored to increase sulfur utilization and alleviate the shuttle of polysulfides. On the other hand, the renaissance of Li metal batteries has spawned some effective strategies, such as controlling Li-ion flux, designing porous current collectors, introducing artificial solid electrolyte interphase (SEI) layers, and using concentrated electrolytes, to suppress the formation of Li dendrites and prolong the lifespan of Li metal anodes.[12-16] Encouragingly, the past few years have witnessed the outpouring of Li-S batteries with improved performance.[4-10]

However, most of the improvements are achieved at the electrode level.[17,18] Integrating the present strategies on sulfur cathodes and Li metal anodes into a battery will face the complicated and tedious battery manufacturing process. Even worse, Li-S batteries are usually fabricated with low sulfur loading

[a] Pen-Tung Sah Institute of Micro-Nano Science and Technology, State Key Laboratory for Physical Chemistry of Solid Surfaces, Collaborative Innovation Center of Chemistry for Energy Materials, National & Local Joint Engineering Research Center for Preparation Technology of Nanomaterials, and College of Chemistry and Chemical Engineering, Xiamen University, Xiamen, Fujian 361005, China.
Email: x.l.fang@xmu.edu.cn; nfzheng@xmu.edu.cn
[b] Fujian Science & Technology Innovation Laboratory for Energy Materials of China, Xiamen, Fujian 361005, China.
[c] CAS Key Laboratory of Carbon Materials, Institute of Coal Chemistry, Chinese Academy of Sciences, Taiyuan 030001, China.
[d] University of Chinese Academy of Sciences, Beijing 100049, China.
†Electronic Supplementary Information (ESI) available. See DOI: 10.1039/x0xx00000x

(< 5 mg_S cm^{-2}), high electrolyte/sulfur (E/S) ratio (> 10 µL mg_S^{-1}), and high negative/positive capacity (N/P) ratio (> 10/1).[17-19] Although some Li-S batteries have been able to deliver high areal capacities under flooded electrolyte conditions, technical analyses clearly indicated that their gravimetric energy densities are difficult to exceed 200 Wh kg^{-1}, far lower than the state-of-the-art LIB.[20,21] Considering that the amount of electrolyte plays a key role in determining the energy density and cost of batteries, low E/S ratio is crucial to creating a competitive Li-S battery.[20-24] An ideal low E/S battery is expected to support the normal operation of high-sulfur-loading cathodes while preventing Li dendrite formation and mitigating the parasitic reactions between Li and electrolyte. Unfortunately, for most high-sulfur-loading batteries, reducing the electrolyte amount inevitably results in severe performance degradation. Consequently, it still remains a challenging task to develop high-energy-density Li-S batteries.[25-29]

To simultaneously overcome the polysulfide shuttling and Li dendrite issues, ion-conductive polymers and ceramics have been investigated as solid electrolytes to replace traditional liquid electrolytes.[30,31] Until now, some intractable problems including low ionic conductivity, the interface problem of electrolyte/electrode, and the inefficiency of solid-state sulfur conversion still hinder the widespread application of solid electrolytes in Li-S batteries, especially in high-sulfur-loading batteries.[32,33] As a kind of quasi-solid electrolytes, gel polymer electrolytes (GPE), also known as the liquid electrolyte packaged within polymer matrix, possess improved ionic conductivity and interfacial compatibility with both cathode and anode.[34-37] Due to the presence of electrolyte solvent, GPE is capable of promoting sulfur conversion at a liquid/solid interface.[25,38-40] Although these features make GPE available for constructing Li-S batteries with high sulfur loading, the plasticization of liquid electrolyte can dramatically reduce the mechanical stabilities of GPE. To address this issue, introducing inorganic nanoparticles (e.g., TiO_2, Al_2O_3, and SiO_2) into the polymer matrix is widely used to reinforce GPE.[30,41-44] However, these inorganic fillers are usually not uniform in morphology or size. Moreover, they tend to aggregate in the polymer matrix and thus result in the phase separation and local inhomogeneity of GPE.[30] It is highly desirable to develop high-quality fillers with rationally designed surface structures and properties to improve the performance of GPE Li-S batteries. In addition, the amounts of electrolyte and metallic Li used in most GPE Li-S batteries are similar to those of liquid-electrolyte Li-S batteries, meaning that the potential of GPE has yet to be tapped.[38-40]

Herein, we report the design and synthesis of titanium-oxo clusters (TOC) reinforced GPE for the construction of low E/S Li-S batteries. Metal-oxo clusters with well-defined structures and uniform characteristics in shape, size, and composition, are considered as an important category of organic-inorganic hybrid materials.[45-48] As with the majority of metal-oxo clusters, TOC is flourishing in terms of new structures and new compositions, but lag behind in new applications.[47] In this work, we show for the first time that TOC is a versatile filler to enhance the mechanical and electrochemical properties of GPE. The designed TOC can significantly promote the film-forming behaviour of polymer matrix, rendering GPE to suppress the polysulfide shuttling and to guide uniform Li deposition. The high-sulfur-loading batteries fabricated with low E/S and N/P ratios demonstrate that the TOC-reinforced GPE has great potential to improve the energy density and cycling stability of Li-S batteries. In addition, this GPE can also be used for fabricating bendable/foldable Li-S batteries.

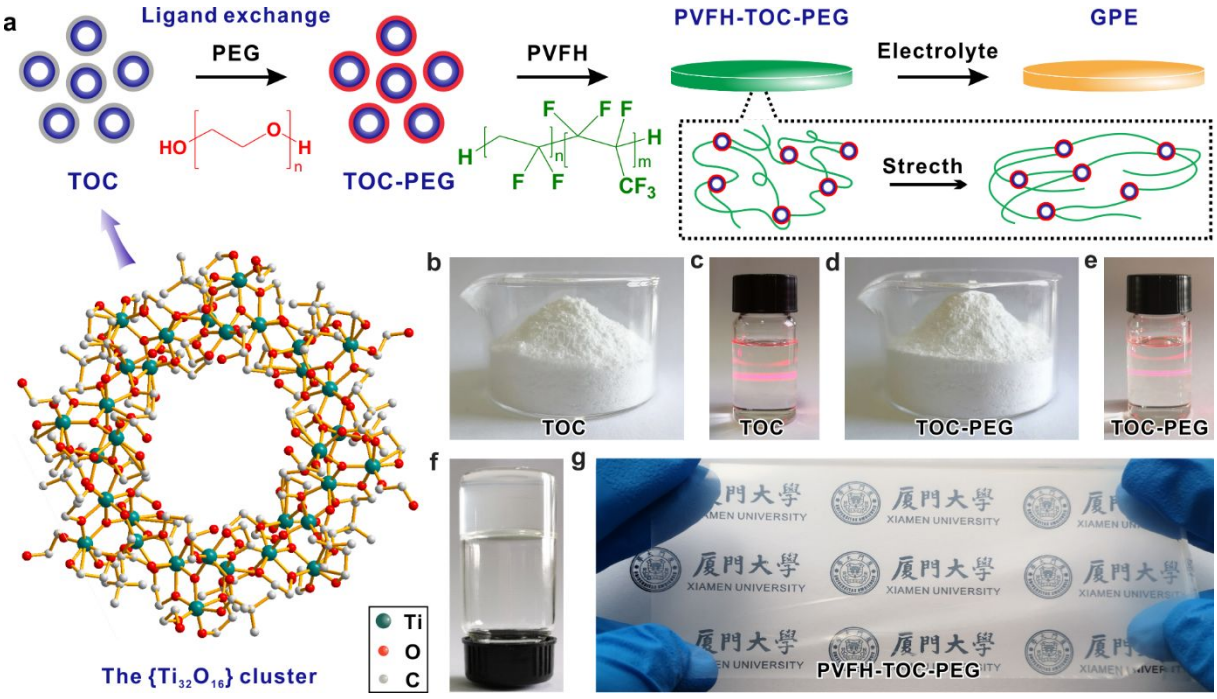

Fig. 1 Synthesis of the TOC-reinforced GPE. (a) Crystal structure of TOC and schematic illustration for the synthesis of the PVFH-TOC-PEG electrolyte. (b) Gram-scale synthesis of TOC. (c) TOC dispersed in CH_2Cl_2. (d) Grams of TOC-PEG obtained by the ligand exchange. (e) TOC-PEG dispersed in CH_2Cl_2. (f) The PVFH-TOC-PEG gel. (g) The PVFH-TOC-PEG membrane.

Results and discussion

Design and synthesis of the TOC-reinforced GPE

As a core component of GPE, the polymer matrix serves as the scaffold to immobilize liquid electrolyte and largely determines the fundamental characteristics of GPE.[34-37] From the viewpoint of the filler-reinforced GPE, controlling the morphology and size of fillers and regulating the filler-polymer interactions are of great importance.[49,50] In these regards, ligand-decorated metal-oxo clusters are expected to surpass the conventionally used fillers (e.g., TOC vs. TiO_2), owing to their unique advantages including uniform structure parameters and precisely manipulated surface functional groups.[47,48] Although metal-oxo clusters with diverse compositions and structures are constantly being created, they have not yet been applied in GPE batteries. To demonstrate their potentials for GPE and high-energy-density Li-S batteries, we chose poly(vinylidene fluoride-co-hexafluoropropylene) (PVFH), an electrochemically stable polymer used commonly in GPE, as the polymer matrix. Our recently reported TOC with a formula of $Ti_{32}O_{16}(OCH_2CH_2O)_{32}(RCOO)_{16}(EGH)_{16}$ (R = *t*-butyl, EGH = -OCH_2CH_2OH) was used as the fillers with controllable surface functionality.[51] The selected TOC has a cyclic $\{Ti_{32}O_{16}\}$ backbone and exhibit a wheel-like shape with a diameter of 2.69 nm and a height of 1.04 nm (for structural details see Fig. 1a and Fig. S1, ESI†). For the GPE Li-S batteries, the $\{Ti_{32}O_{16}\}$ clusters have several inherent advantages: (i) their synthesis process is convenient, inexpensive, and easily scalable (Fig. 1b);[51] (ii) they are highly dispersible in organic solvents (Fig. 1c); (iii) they are stable in the ether-based Li-S electrolytes (Fig. S2, ESI†); (iv) their surface EGH ligands are highly exchangeable with other alcohols, making the post-functionalization of the clusters easy to achieve.[51]

The preparation procedure of the TOC-enhanced GPE is schematically depicted in Fig. 1a. In a typical synthesis, the EGH ligands of the $\{Ti_{32}O_{16}\}$ clusters were firstly exchanged with polyethylene glycols (PEG-400) in dichloromethane (CH_2Cl_2) at room temperature (Fig. 1d and Fig. S3, ESI†). We chose PEG for functionalization because the Li^+-conductive PEG can influence the crystallinity and porosity of PVFH,[30,37] which is expected to improve the dispersion behaviour of TOC in PVFH, as well as the ion conductivity and mechanical performance of the PVFH-TOC composite (*vide infra*). Note that the excellent dispersibility of the $\{Ti_{32}O_{16}\}$ clusters was well inherited by the PEG-decorated $\{Ti_{32}O_{16}\}$ clusters (TOC-PEG). The Tyndall effect demonstrated the colloidal nature of the TOC-PEG dispersion (Fig. 1e). Next, the CH_2Cl_2 solution of TOC-PEG was mixed with a PVFH acetonic solution at a TOC-PEG/PVFH ratio of 5/95 (weight/weight) under vigorous stirring. The homogeneous mixture (Fig. 1f) was further cast on a polytetrafluoroethylene plate, and a thin PVFH-TOC-PEG membrane was obtained after curing process. The PVFH-TOC-PEG membrane is uniform and optically transparent (Fig. 1g), which contrasts sharply with the opaque membrane made from the P25 TiO_2 nanoparticles filled PVFH (Fig. S4, ESI†). The characteristic bonds of PVFH, TOC, and PEG can be identified in the Fourier transform infrared (FTIR) spectrum of the PVFH-TOC-PEG membrane (Fig. S5, ESI†). Finally, in an Ar-filled glovebox, the tailored PVFH-TOC-PEG membrane was soaked into the electrolyte (1 M bis(trifluoromethanesulfonyl)imide lithium (LiTFSI) in a mixture of 1,2-dimethoxyethane/1,3-dioxolane (DME/DOL, vol/vol = 1/1) with 2 wt% $LiNO_3$), yielding a GPE membrane with an electrolyte uptake of 300% (i.e., liquid electrolyte/PVFH-TOC-PEG = 3/1, weight/weight).

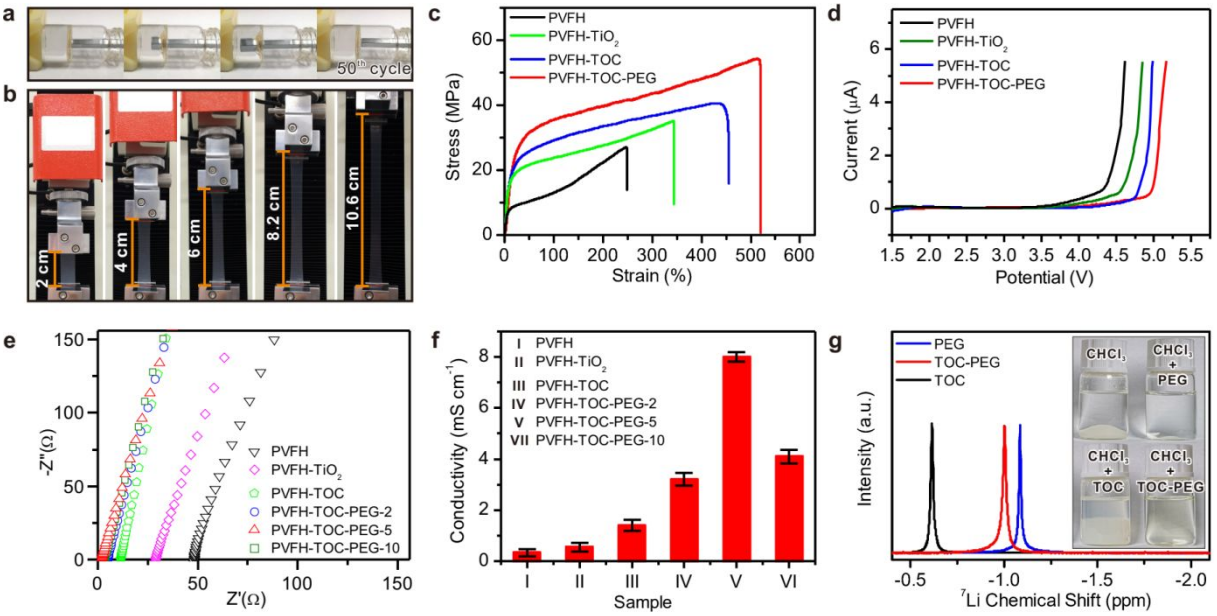

Fig. 2 Characterization of the TOC-reinforced GPE. (a) The PVFH-TOC-PEG electrolyte pressed with a metal bar. (b) Stress-strain measurement of the PVFH-TOC-PEG membrane. (c) Stress-strain curves of the PVFH-based membranes. (d) ESW of the PVFH-based GPE. (e) EIS measurements of the PVFH-based GPE. (f) Li^+ conductivities of the PVFH-based GPE (abbreviations: PVFH-TOC-PEG-2, -5, and -10 are the PVFH-TOC-PEG with 2, 5, and 10 wt% of TOC-PEG, respectively). (g) ^7Li NMR spectra of the deuterated chloroform solution of LiTFSI with different additives. Inset: LiTFSI with different solvents.

Mechanical and electrochemical properties

The fabricated PVFH-TOC-PEG electrolyte appears clear and transparent, as shown in the optical images (Fig. 2a and Fig. S6, ESI†). This GPE is mechanically tough with a rubbery-like behaviour and has a high capacity to recover from large deformation. For instance, the morphology of the GPE was well maintained after being pressed with a metal bar for 50 times (Fig. 2a). The favourable mechanical strength of the PVFH-TOC-PEG electrolyte arises from its enhanced polymer matrix. We found that the PVFH-TOC-PEG membrane could be stretched to 5.2 times its original length without rupture (Fig. 2b). For comparison, PVFH, PVFH with 5 wt% of P25 TiO_2 (PVFH-TiO_2), and PVFH with 5 wt% of the $\{Ti_{32}O_{16}\}$ clusters (PVFH-TOC) were used as the reference samples. These membranes were also tested with a strain-stress mechanical tester (Fig. 2c). The maximum stress and strain values of the membranes increased following the order of PVFH < PVFH-TiO_2 < PVFH-TOC < PVFH-TOC-PEG (Table S1), indicating enhancement of the mechanical properties of PVFH by filler addition. Compared with TiO_2, the intermolecular hydrogen bonding effect of PVFH (C-F bands) and TOC (-O-H bands of EGH or PEG) helps to increase the interaction between PVFH and TOC fillers (Fig. S7, ESI†),[37] which is reflected by the melting points of the PVFH-based membranes (141 °C for PVFH-TiO_2, 144 °C for PVFH-TOC, and 153 °C for PVFH-TOC-PEG) (Fig. S8, ESI†). These results reveal that the PEG functionalization is beneficial to enhance the reinforcing effect of TOC on PVFH. Additionally, it is worth pointing out that the PVFH-TOC-PEG membrane also exhibited good mechanical strength after soaking with the electrolyte (Fig. S9, ESI†).

In addition to mechanical properties, the electrochemical performance of GPE can also be remarkably enhanced by introducing TOC-PEG. The electrochemical stability window (ESW) of the PVFH-TOC-PEG electrolyte is stable up to ~5.0 V *versus* Li^+/Li, higher than those of the PVFH-TOC (4.8 V), PVFH-TiO_2 (4.6 V), and PVFH (4.3 V) electrolytes (Fig. 2d). The expanded ESW suggests that TOC-PEG has the potential to improve the PVFH-based GPE for recently emerging high-voltage cathode materials.[52] The ionic conductivities of the PVFH-based GPE were measured with electrochemical impedance spectroscopy (EIS) (Fig. 2e and 2f). The PVFH-TOC-PEG electrolyte has a high Li^+ conductivity of 8 x 10^{-3} S cm^{-1} at 25 °C, ~24 times higher than that of the PVFH electrolyte (3.3 x 10^{-4} S cm^{-1}). This value is slightly lower than liquid electrolytes, but considerably higher than those of many other GPE, and is enough to support Li-S battery operating at room temperature.[39,40] As show in Fig. 2f, the introduction of fillers facilitates the ion transport in the GPE, especially for the case of TOC-PEG. The Li^+ conductivity of the GPE increases with the TOC-PEG content (see the cases of 0 wt%, 2 wt%, and 5 wt%). However, excessive addition of TOC-PEG would decrease the Li^+ conductivity (see the case of 10 wt%), as partial TOC-PEG can be precipitated from the mixture of CH_2Cl_2/acetone under high TOC-PEG content conditions (Fig. S10, ESI†). Moreover, the activation energy of the PVFH-TOC-PEG electrolyte calculated based on the temperature-

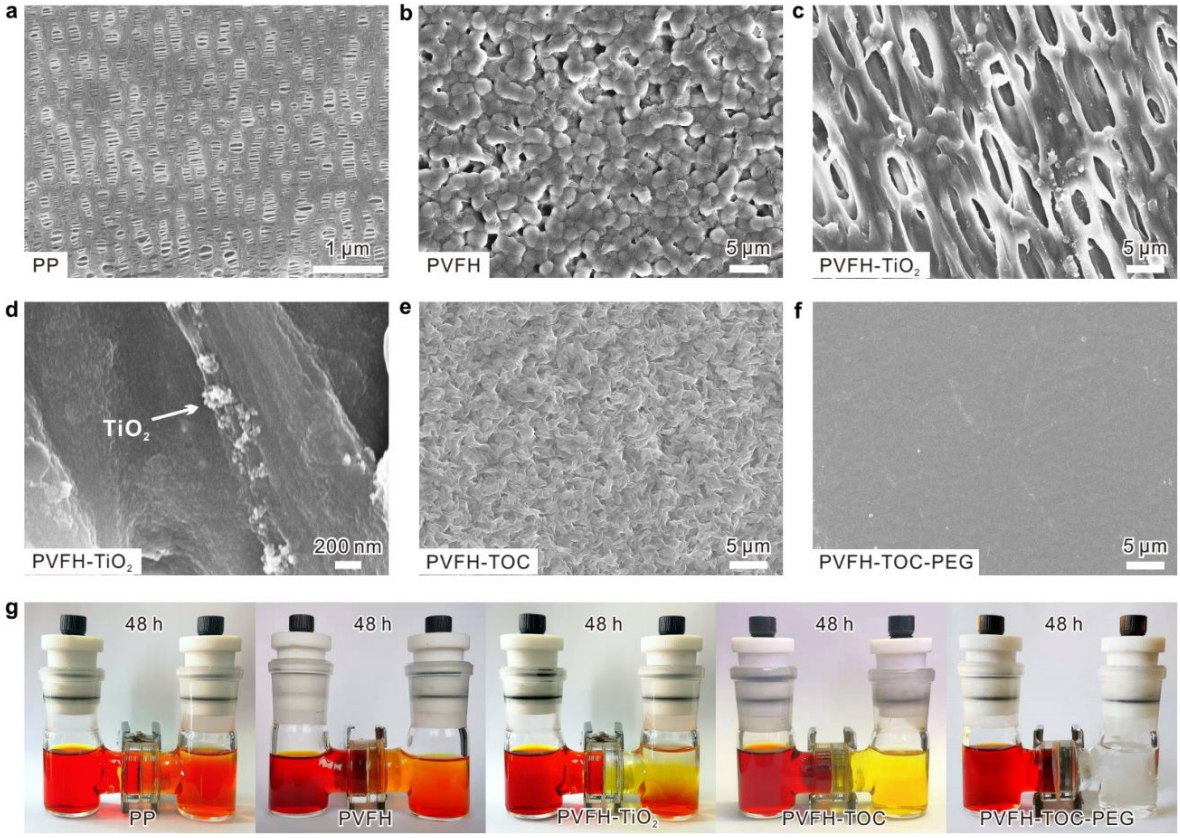

Fig. 3 Polysulfide-blocking capabilities of the PVFH-based GPE. (a-f) SEM images of (a) PP, (b) PVFH, (c) and (d) PVFH-TiO_2, (e) PVFH-TOC, and (f) PVFH-TOC-PEG membranes. (g) Polysulfide permeation tests for PP and GPE.

dependent ionic conductivity is ~0.13 eV (Fig. S11, ESI†), representing a low barrier for Li^+ transport.[34]

The reasons for the high Li^+ conductivity of the PVFH-TOC-PEG electrolyte are two-fold. (i) TOC-PEG can increase the amorphous regions of PVFH, which is beneficial for improving the Li^+ mobility in GPE.[32] The X-ray diffraction (XRD) measurements showed that the crystallinity of PVFH was decreased by adding the fillers, and the crystallinities of the PVFH-based polymers decreased in the order of PVFH > PVFH-TiO_2 > PVFH-TOC > PVFH-TOC-PEG (Fig. S12, ESI†). (ii) The PEG functionalization allows TOC-PEG to serve as Li^+-solvating fillers that increase the Li^+ conductivity. It is well-known that PEG is Li^+ conductive and able to solvate Li^+.[32] Interestingly, TOC-PEG remains these features of PEG. As shown in the inset of Fig. 2g, LiTFSI was partially soluble in chloroform ($CHCl_3$), but dissolved completely after a certain amount of PEG-400 was added. When LiTFSI was added into the TOC/$CHCl_3$ and TOC-PEG/$CHCl_3$ solutions, respectively, most of LiTFSI did not dissolve in TOC/$CHCl_3$, whereas all LiTFSI were dissolved in TOC-PEG/$CHCl_3$ and formed a transparent solution. The ^7Li NMR spectra of LiTFSI with different additives also reveal that the interaction between Li^+ and TOC-PEG is higher than the interaction of Li^+ and TOC (Fig. 2g). Therefore, the TOC-PEG promoted Li^+ solvation behaviour mainly stems from the surface PEG ligands of TOC-PEG.

Blocking the migration of polysulfides

In liquid-electrolyte Li-S batteries, the shuttling of the dissolved polysulfides (Li_2S_n, $4 \le n \le 8$) between two electrodes is a troublesome problem, as the highly porous polypropylene (PP) separator (Fig. 3a) cannot block the migration of polysulfides from cathode to anode.[1-3] Compared with liquid electrolytes, the quasi-solid feature endows GPE with an obvious advantage in suppressing the polysulfide shuttling.[38-40] To investigate the relation between the polysulfide-blocking capabilities of GPE and the microstructures of the polymer matrixes, the PVFH-based membranes were characterized with scanning electron microscope (SEM). As shown in Fig. 3b, the surface of PVFH is full of the interconnected bead-like particles. These irregularly arranged particles create a number of micron-scale pores. In the case of PVFH-TiO_2, fiber-like PVFH forms a porous network, and aggregated TiO_2 nanoparticles can be observed on the surface of PVFH (Fig. 3c and 3d). In contrast, PVFH-TOC has a macropore-free surface but with continuous wrinkles (Fig. 3e). More impressively, a highly dense, smooth, and pinhole-free surface was observed in PVFH-TOC-PEG (Fig. 3f). Small angle X-

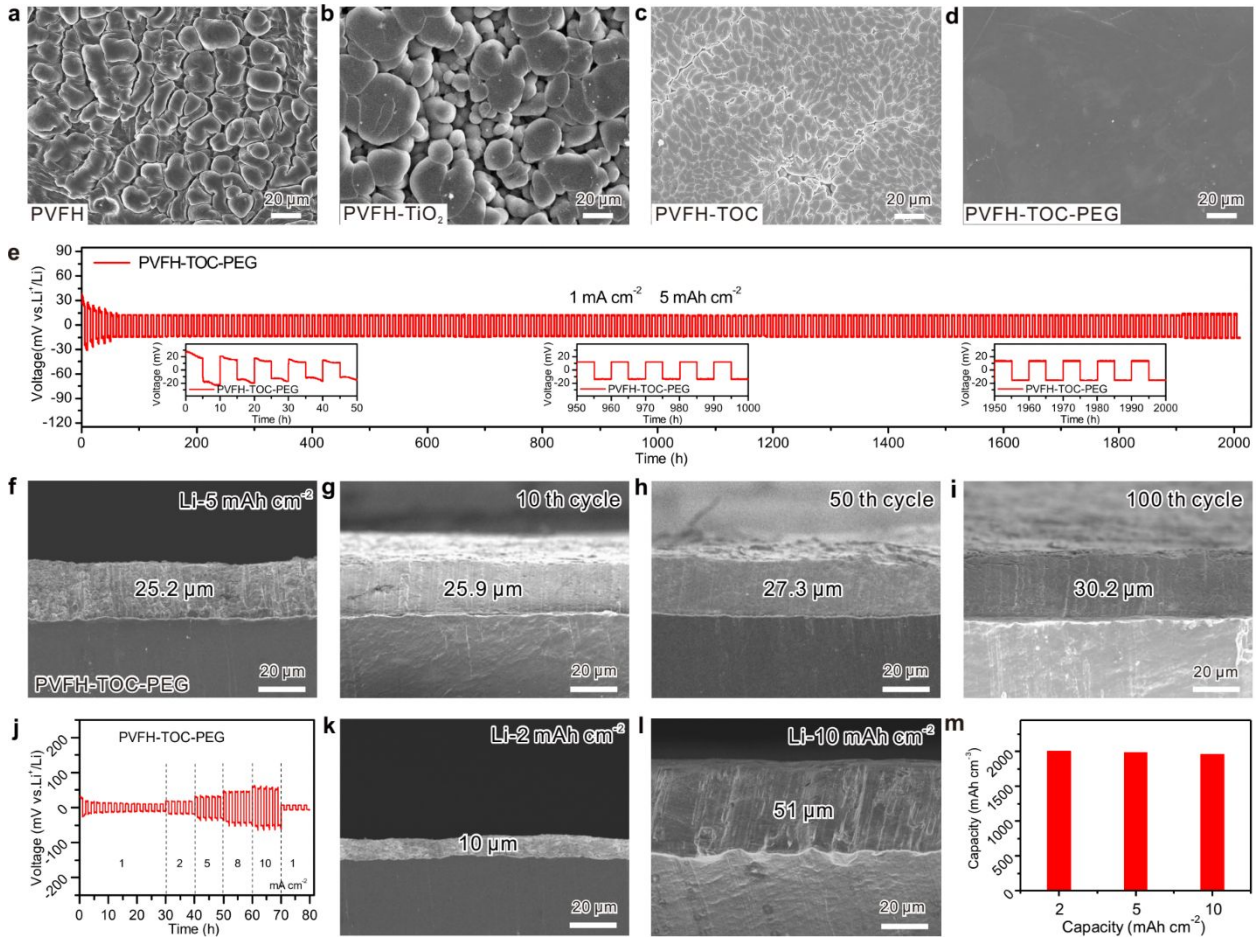

Fig. 4 Characterization of Li|GPE|Li cells. (a-d) Top-view SEM images of Li deposition layer (5 mAh cm^{-2} Li) in (a) PVFH, (b) PVFH-TiO_2, (c) PVFH-TOC, and (d) PVFH-TOC-PEG cells. (e) Voltage profile of the PVFH-TOC-PEG cell at 1 mA cm^{-2} and 5 mAh cm^{-2}. Inset: representative voltage profiles. (f-i) Cross-section SEM images of Li deposition layer (5 mAh cm^{-2} Li) in PVFH-TOC-PEG cell after 1, 10, 50 and 100 stripping/plating cycles at 1 mA cm^{-2}. (j) Rate capability of the PVFH-TOC-PEG cell. (k and l) Cross-section SEM images of Li deposition layer in the PVFH-TOC-PEG cell after 1 stripping/plating cycle. (m) Volumetric capacities of Li deposition layers in the PVFH-TOC-PEG cells.

ray scattering measurement demonstrates that the TOC-PEG in the PVFH-TOC-PEG membrane is highly dispersed (Fig. S13, ESI†). When TOC-PEG was replaced with equal amounts of PEG-400 (i.e., 5 wt%), the volatilization of liqiud PEG-400 during the drying process resulted in a membrane with a macroporous surface (Fig. S14, ESI†). Obviously, the use of TOC-PEG is critical to forming a high-quality PVFH membrane.

Note that the morphology of the polymer matrix can affect the density of GPE. The densities of the PVFH, PVFH-TiO_2, PVFH-TOC, and PVFH-TOC-PEG GPE are 1.31, 1.33, 1.46, and 1.53 g cm^{-3}, respectively, indicating that PVFH-TOC-PEG GPE is more compact than the other three GPE. The permeability of polysulfides through GPE was further examined using Li_2S_6 as a model polysulfide.[10] In five U-type glass cells, the tetrahydrofuran (THF) solution of Li_2S_6 (0.1 M) and pure THF were separated by the PP separator and different PVFH-based GPE, respectively (Fig. 3g). In the PP-separated glass cell, plenty of Li_2S_6 migrated from the Li_2S_6 solution side to the THF side after 48 hrs. When GPE was used, the migration of Li_2S_6 was obviously suppressed. Benefiting from the dense polymer matrix, no Li_2S_6 migration was observed after 48 hrs in the case of PVFH-TOC-PEG, suggesting that the TOC-reinforced GPE would be effective in enhancing the cycling stability of sulfur cathodes.

Guiding uniform lithium deposition

With the development of sulfur cathodes, the cycling life of Li-S batteries, especially under lean electrolyte conditions, is mainly restricted by the stability of Li metal anodes, which is associated with the uneven Li deposition induced dendrite formation and electrolyte consumption.[12,13] To demonstrate that TOC-PEG can be useful to improve the capability of GPE in regulating Li deposition behavior, Li|GPE|Li symmetrical cells were assembled with commercial Li foils and charged/discharged at 1 mA cm^{-2}. After 1 stripping/plating cycle, the morphology of the Li deposition layer with 5 mAh cm^{-2} Li was measured by *ex-situ* SEM. Porous Li films composed of irregular granulars were observed in the PVFH and PVFH-TiO_2 symmetrical cells (Fig. 4a and 4b). When TOC was used as the filler, the small-sized Li granulars were packed closely together and formed a relatively dense film (Fig. 4c). In sharp contrast, a highly dense and dendrite-free Li film was obtained in the PVFH-TOC-PEG cell (Fig. 4d), implying that the PVFH-TOC-PEG electrolyte guided a uniform Li deposition. During the repeated charge/discharge process, the PVFH-TOC-PEG symmetrical cell showed an outstanding stability for 2000 hrs (200 cycles) with a stable voltage hysteresis around 26 mV (Fig. 4e), better than many of the quasi-solid electrolyte derived symmetrical cells (Table S2). The cross-section SEM images of the PVFH-TOC-PEG cell also clearly indicate that the Li deposition layers obtained after different stripping/plating cycles are highly dense (Fig. 4f-4i). From 1 to 100 cycles, the thickness of 5 mAh cm^{-2} Li was increased from 25.2 to 30.2 μm.

Considering that high current densities are desirable for high-sulfur-loading batteries, the Li|GPE|Li cells were further charged/discharged from 1 to 10 mA cm^{-2} (Fig. 4j). The voltage

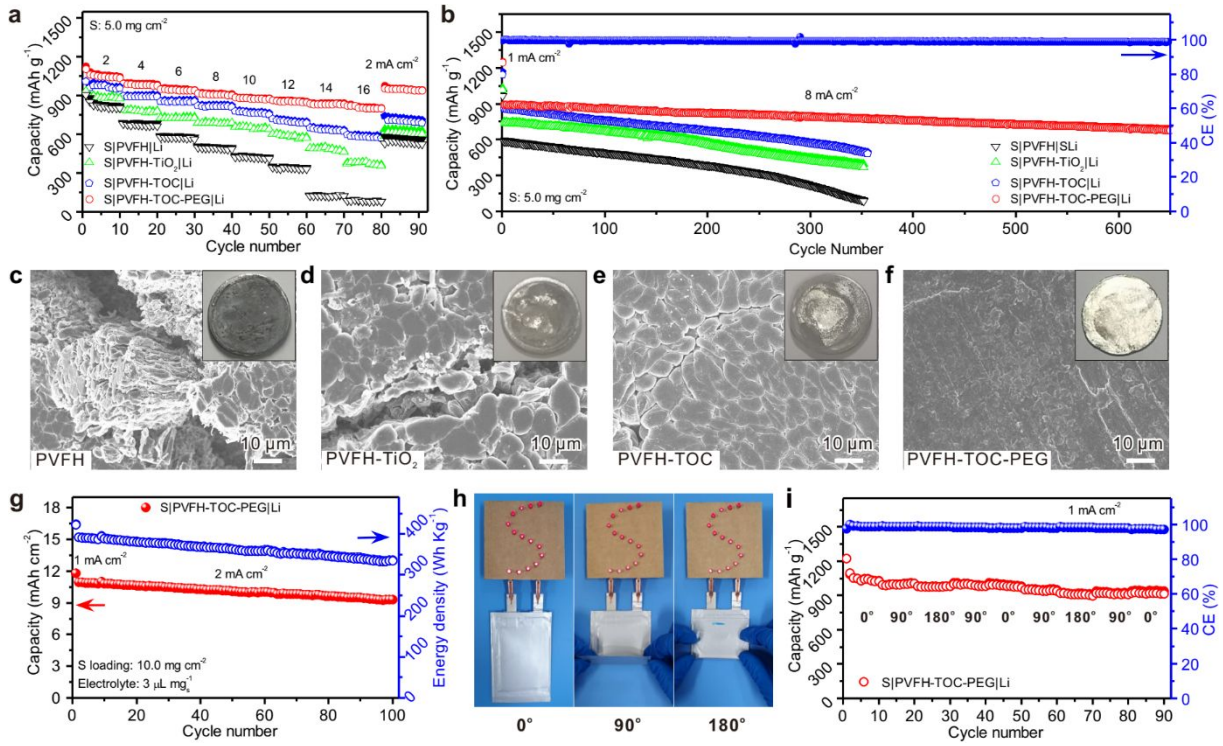

Fig. 5 Electrochemical performance of GPE Li-S batteries. (a) Rate capabilities of the GPE Li-S cells with an E/S ratio of 6 μL mg_S^{-1}. (b) Cycling performance of the GPE Li-S cells at 8 mA cm^{-2}. (c-f) Optical and SEM images of the Li metal anodes after the cycling tests: (c) the S|PVFH|Li cell, (d) the S|PVFH-TiO_2|Li cell, (e) the S|PVFH-TOC|Li cell, and (f) the S|PVFH-TOC-PEG|Li cell. (g) Cycling performance of the S|PVFH-TOC-PEG|Li cell with 10.0 mg cm^{-2} of sulfur, 3 μL mg_S^{-1} of E/S ratio, and 1/1 of N/P ratio. (h and i) Flexible S|PVFH-TOC-PEG|Li battery evaluated under different conditions.

hysteresis of the PVFH-TOC-PEG cell increases with increasing current density and keeps steady at 10 mA cm^{-2}, which is obviously lower than those of the PVFH, PVFH-TiO_2, and PVFH-TOC cells (Fig. S15, ESI†). More importantly, when used the PVFH-TOC-PEG electrolyte, uniform Li deposition can be achieved even at a high Li plating areal capacity. As shown in Fig. 4f, 4k, and 4l, with Li plating areal capacity increased from 2, 5 to 10 mAh cm^{-2}, the Li deposition layer had kept its "dense" feature. Notably, the volumetric capacities of the Li deposition layers with 2, 5, and 10 mAh cm^{-2} of Li were calculated to be 2000, 1980, and 1960 mAh cm^{-3}, respectively (Fig. 4m). These values are very close to the theoretical capacity of Li (2060 mAh cm^{-3}). The good cycling stability of the PVFH-TOC-PEG cell at a current density of 4.5 mA cm^{-2} and a Li capacity of 2.5 mAh cm^{-2} further suggests that the combination of PVFH-TOC-PEG electrolyte and Li metal has the capability to meet the requirements of high-sulfur-loading batteries (Fig. S16, ESI†). In the PVFH-TOC-PEG cell, the uniform Li deposition is attributed to the highly humongous polymer matrix of GPE, which is capable of homogenizing the Li^+ flux at the GPE/Li interface.[12,13] In addition, the Li^+ transference number of the PVFH-TOC-PEG electrolyte (0.77) is higher than those of the PVFH-TOC (0.72), PVFH-TiO_2 (0.53), and PVFH (0.41) electrolytes (Fig. S17, ESI†). High Li^+ transference number can effectively reduce the Li^+ concentration polarization near Li metal surface, which is helpful for suppressing the dendrite formation.[32] Since dense Li deposition minimizes the contact area between Li metal and electrolyte so as to reduce the consumptions of both Li and electrolyte, the PVFH-TOC-PEG electrolyte is applicable for constructing Li-S batteries with low E/S and N/P ratios.[53]

Application in high-energy-density Li-S Batteries

To explore the feasibility of the TOC-reinforced GPE in lean-electrolyte Li-S batteries, high-sulfur-loading C/S cathodes with 67.0 wt% and 5.0 mg cm^{-2} of sulfur were prepared using commercial carbon black (CB) as the sulfur host (Fig. S18, ESI†), and the cathode slurry was fabricated using the mixture of PVFH-TOC-PEG and LiTFSI as a Li^+ conducting binder (for details see experimental section). S|GPE|Li coin cells with a low E/S ratio of 6 μL mg_S^{-1} were assembled by pairing the CB/S cathodes with the PVFH-based GPE and commercial Li foils. It needs to be emphasized that the GPE cells assembled in this work did not use separator and extra liquid electrolytes, and the E/S ratios were calculated based on the Li-S electrolyte contained in the PVFH-based GPE. The capacities and rate capabilities of the S|GPE|Li cells were measured by galvanostatic charge/discharge at current densities varying from 2 to 16 mA cm^{-2} (Fig. 5a and Fig. S19, ESI†). In the first cycle at 2 mA cm^{-2}, the discharge capacity of the S|PVFH-TOC-PEG|Li cell calculated based on the mass of sulfur was as high as 1103 mAh g^{-1}, higher than those of the S|PVFH-TOC|Li (1006 mAh g^{-1}), S|PVFH-TiO_2|Li (935 mAh g^{-1}), and S|PVFH|Li (907 mAh g^{-1}) cells. When the current density was increased to 16 mA cm^{-2}, the S|PVFH-TOC-PEG|Li cell still delivered a high capacity of 802 mAh g^{-1} (Fig. 5a). In striking contrast, the capacities of the S|PVFH-TOC|Li, S|PVFH-TiO_2|Li, and S|PVFH|Li cells at 16 mA cm^{-2} were only 577, 379, and 82 mAh g^{-1}, respectively. The capacities and rate capabilities of these cells correlate well with the Li^+ conductivities and Li^+ transference numbers of the GPE they contain.

Since the PVFH-TOC-PEG electrolyte can simultaneously suppress the polysulfide shuttling and Li dendrite formation, the S|PVFH-TOC-PEG|Li cell with an E/S ratio of 6 μL mg_S^{-1} possesses an enhanced long-term cycling stability. As shown in Fig. 5b and Fig. S20 (ESI†), this cell exhibited an initial capacity of 890 mAh g^{-1} at 8 mA cm^{-2}. After 650 cycles, a high discharge capacity of 680 mAh g^{-1} was retained. The corresponding capacity retention is 76.4%, representing a low capacity decay of 0.036% per cycle. During the cycling test, the charge-transfer resistance of the S|PVFH-TOC-PEG|Li cell increased with the capacity degradation (Fig. S21, ESI†). The capacity decay of the S|PVFH-TOC-PEG|Li cell was mainly due to the parasitic reaction occurred at the GPE-Li interface, as the slow increase in thickness of Li deposition layer was observed in Fig. 4f-4i). When the PVFH-TOC-PEG electrolyte was replaced with the reference GPE, rapid capacity decay was observed. The capacities of 493, 368, and 95 mAh g^{-1} were achieved for the S|PVFH-TOC|Li, S|PVFH-TiO_2|Li, and S|PVFH|Li cells after 350 cycles, respectively (Fig. 5b). After the cycling test, the cells were disassembled to observe the cycled Li metal anodes. Impressively, the Li foils in the S|PVFH-TOC-PEG|Li and S|PVFH-TOC|Li cells were relatively dense, whereas serious corrosion and pulverization of Li foils were observed in both the S|PVFH|Li and S|PVFH-TiO_2|Li cells (Fig. 5c-5f).

Considering the electrolyte content can influence the performance of Li-S batteries, the E/S ratio of the S|PVFH-TOC-PEG|Li cell with 5 mg cm^{-2} of S was further reduced from 6 to 4.5 μL mg_S^{-1}. The resulting cell exhibited a discharge capacity of 752 mAh g^{-1} after 100 cycles at 8 mA cm^{-2}, indicating that PVFH-TOC-PEG electrolyte has the potential to improve the performance of lean-electrolyte Li-S batteries (Fig. S22, ESI†). The cycling stability of the S|PVFH-TOC-PEG|Li cell is superior to most of the lean-electrolyte Li-S batteries reported recently, and even better than some flooded-electrolyte Li-S batteries (Table S3).[26-28] The remarkably improved electrochemical performance of S|PVFH-TOC-PEG|Li cell can be attributed to the unique functions of TOC-PEG: a) the PEG-modified surface and good compatibility with PVFH make TOC-PEG feasible to increase the Li^+ conductivity of PVFH-TOC-PEG, leading to improvements in capacity and rate performance; b) the dense and compact polymer matrix formed by adding TOC-PEG allows PVFH-TOC-PEG to serve as an efficient physical barrier to suppress polysulfide shuttling, which effectively reduce the capacity fading of sulfur cathode and the side reactions between polysulfides and Li metal anode; c) the highly humongous polymer matrix and high Li^+ transference number achieved by adding TOC-PEG enable PVFH-TOC-PEG to induce dendrite-free lithium deposition, and thus improve the cycling stability of Li metal anode.

To further reveal the potential of the TOC-reinforced GPE in improving the energy density of Li-S batteries, a CB/S cathode with 10.0 mg cm^{-2} of sulfur and a pressed Li foil with a thickness of ~80 μm (Fig. S23, ESI†) were employed to construct a S|PVFH-TOC-PEG|Li cell with a low E/S ratio of 3 μL mg_S^{-1} and a low N/P ratio of 1/1. As shown in Fig. 5g, this cell delivered a high areal capacity of 11.8 mAh cm^{-2} at 1 mA cm^{-2}. Based on the total weight of cathode current collector, CB/S cathode, GPE, and Li metal anode, the gravimetric energy density (E_g) and the gravimetric power density of the S|PVFH-TOC-PEG|Li cell were calculated to be 423 Wh kg^{-1} and 31 W kg^{-1}, respectively. Remarkably, this cell can be repeatedly

charged/discharged with a good cycling stability. A high E_g of 334 Wh kg^{-1} was maintained after 100 cycles at 2 mA cm^{-2} (Fig. 5g and Fig. S24, ESI†). Compared with the initial E_g at 2 mA cm^{-2} (391 Wh kg^{-1}), the capacity retention is ca. 85.4%. More importantly, the E_g and cycling stability of a large-areal S|PVFH-TOC-PEG|Li pouch cell agree well with those of the S|PVFH-TOC-PEG|Li coin cell (Fig. S25, ESI†). Considering that the electrodes of the S|PVFH-TOC-PEG|Li cell are fabricated based on the commercial materials (i.e., CB and Li foil), the E_g and cycling performance achieved in this work represents a big step toward high-energy-density Li-S batteries (Fig. S26, ESI†).[3,17-21]

With development of flexible electronics, bendable/foldable batteries are becoming an important direction of battery technology.[54-58] The favorable mechanical and electrochemical properties make the TOC-reinforced GPE a promising candidate for constructing bendable/foldable Li-S batteries. As a demonstration, we further investigated the flexibility of the soft packed S|PVFH-TOC-PEG|Li battery. The optical images shows that the fabricated battery can normally power light-emitting diode (LED) lamps under different deformations, such as 90-degree bend and 180-degree fold (Fig. 5h). The battery with different deformations was further tested by the continuously charged/discharged at 1 mA cm^{-2}. As expected, the charge/discharge curves and internal resistances of the battery under the flat, bent, and folded states are very close (Fig. S27 and S28, ESI†). After 90 cycles at 1 mA cm^{-2}, the battery exhibited a discharge capacity of 916 mAh g^{-1} (Fig. 5i). Compared with the discharge capacity obtained before bending, 90% of capacity was retained after the bending tests. Encouraged by the recent progress in flexible electrodes,[54-58] we believe that the TOC-reinforced GPE has a good prospect in bendable/foldable batteries.

Conclusions

In summary, we have put forward a new concept of the TOC-reinforced GPE to construct high-energy-density Li-S batteries. The dilemma "high E/S ratio and low energy density" faced by liquid-electrolyte Li-S batteries can be readily tackled by using the TOC-reinforced GPE to stabilize high-sulfur-loading cathodes and Li metal anodes under low E/S and N/P ratios. Beyond using TOC as uniform fillers, we demonstrated that taking the advantage of TOC in surface modification is crucial for enhancing the performance of GPE. The developed PVFH-TOC-PEG electrolyte is not only conducive to improve the energy density of Li-S batteries, but also suitable for flexible devices, offering useful insights into the development of advanced Li-S batteries. In addition, it is worth noting that many of the reported TOC are water-unstable. The successful application of TOC in the water-free circumstance provided by batteries is also an inspiration for the water-unstable cluster materials. We believe the combination of electrolytes and ligand-decorated metal-oxo clusters will open new opportunities for both electrochemical energy storage and materials chemistry.

Experimental

Chemicals and materials

Pivalic acid (98%), tetrabutyl titanate ($Ti(OBu)_4$, 99%), ethylene glycol, THF, CH_2Cl_2, $CHCl_3$, ethyl ether, N, N-dimethylformamide (DMF), acetone, PEG-400, P25 TiO_2, and sublimed sulfur were purchased from Sinopharm Chemical Reagent Co., Ltd.. PVFH and polyacrylonitrile (PAN) were supplied by Aldrich. Lithium sulfide (Li_2S) was purchased from Alfa Aesar. Li_2S_6 was synthesized by reacting Li_2S with S.[10]

Preparation of TOC

TOC was synthesized according to our previous work with slight modifications.[51] Typically, 24 g of pivalic acid and 12.5 mL of $Ti(OBu)_4$ were added to 200 mL of ethylene glycol. After magnetic stirring for 5 min at room temperature, the turbid mixture was sealed in a Teflon-lined stainless steel autoclave and heated at 100 °C for 24 hrs. The resulting white TOC crystals were collected and washed with anhydrous THF for three times, and finally dried under vacuum at room temperature. Note that the storage and use of TOC powder/dispersion should be performed in a dry environment.

Preparation of TOC-PEG

TOC-PEG was synthesized via the ligand exchange method. 5 g of TOC was dissolved in 50 mL of CH_2Cl_2 and formed a homogeneous solution. After the addition of 7 mL of PEG-400, the solution was further stirred at room temperature for 2 hrs. The obtained TOC-PEG crystals were washed with anhydrous THF for three times to remove the residual PEG and EGH ligands. The purified TOC-PEG was re-dispersed in CH_2Cl_2 with a concentration of 100 mg mL^{-1}.

Preparation of the PVFH-TOC-PEG electrolyte

0.95 g of PVFH was added to 6 mL of acetone and stirred at 60 °C for 5 hrs. Then, 0.5 mL of the TOC-PEG CH_2Cl_2 dispersion was added and stirred at 30 °C for 0.5 hr. The mixture of PVFH and TOC-PEG was cast on a polytetrafluoroethylene plate to form the PVFH-TOC-PEG membrane (~30 μm in thickness). After vacuum-drying at 60 °C for 12 hrs, the PVFH-TOC-PEG membrane was transferred into an Ar-filled glovebox and immersed in a certain amount of Li-S electrolyte for 12 hrs, resulting in the PVFH-TOC-PEG electrolyte. The PVFH-TiO_2 and PVFH-TOC electrolytes were prepared according to the same procedure.

Fabrication of CB/S cathodes

The CB/S composite was prepared by the melt diffusion method.[10] The cathode slurry was obtained by mixing the CB/S composite, CB, PVFH-TOC-PEG, and LiTFSI with a weight ratio of 80:10:8:2 in anhydrous DMF. The as-obtained slurry was then coated onto carbon coated Al foils (12 mm in diameter), resulting in the CB/S cathodes with 67 wt% and 5.0 mg cm^{-2} of sulfur. To further increase the areal sulfur loading (e.g., 10.0 mg cm^{-2}), a lightweight carbon nanofiber paper (~1.0 mg cm^{-2}) was chosen as cathode current collector (CCC). The PAN nanofiber paper obtained by the electrospinning technique was used as the precursor for the preparation of the carbon nanofiber papers. The use of carbon nanofiber paper did not affect the capacity or cycling stability of GPE Li-S batteries (Fig. S29, ESI†).

Characterization

The SEM images were obtained with Zeiss SIGMA. Mechanical testing was carried out on an Instron 5565 testing stain with a strain rate of 5 cm min^{-1}. XRD analysis was performed on a Rigaku Ultima IV. FTIR spectra were measured using a Nicolet iS50 FTIR Spectrometer (Thermo Fisher). Differential scanning calorimetry curves was obtained with a DSC-Q2000 (TA Instruments) at a heating and cooling ramp rate of 10 ^oC min^{-1}. Thermogravimetric analysis was performed on a TGA-SDTA851 (Mettler-Toledo) with a heating rate of 10 ^oC min^{-1} under N_2 atmosphere.

Electrochemical measurements

The ionic conductivities, ESW, and Li^+ transference numbers of GPE were calculated based on the EIS, linear sweep voltammogram, and potentiostatic polarization measurements, respectively. The Li|GPE|Li symmetrical cells and Li-S full cells were assembled in an Ar-filled glovebox (<1 ppm of O_2). Commercial Li foils (0.6 mm in thickness) or pressed Li foils (80 μm in thickness) were used as Li metal anodes. The diameters of the Li foils used in the coin cells with 5.0 and 10.0 mg cm^{-2} of sulfur are 16 mm and 12 mm, respectively. The GPE used in the coin cells with 5.0 and 10.0 mg cm^{-2} of sulfur are always 16 mm in diameter, which are composed of 10 mg of the PVFH-based polymer and 30 μL of Li-S electrolyte. The soft packed battery was assembled with a CB/S cathode (51 mm × 66 mm), a PVFH-TOC-PEG electrolyte (53 mm × 68 mm), and a Li foil (51 mm × 66 mm). The performances of the coin cells and the soft packed battery were measured with a LAND CT2001A cell test instrument. The gravimetric energy density of the Li-S coin cell was calculated based on the equation $E_g = CV/(m_{CCC} + m_{cathode} + m_{anode} + m_{GPE})$, where C is the discharge capacity of cathode; V is the average output voltage; m_{CCC}, $m_{cathode}$, m_{anode}, and m_{GPE} are the weights of the cathode current collector, C/S cathode, Li foil, and PVFH-TOC-PEG electrolyte, respectively.

Conflicts of interest

There are no conflicts to declare.

Acknowledgements

The authors acknowledge the support from the National Key R&D Program of China (2017YFA0207302), the NSF of China (21731005, 21420102001, 21721001, 21801213), and the Fundamental Research Funds for the Central Universities (20720160080, 20720180026).

Notes and references

1 A. Manthiram, Y. Fu, S. H. Chung, C. Zu and Y. S. Su, *Chem. Rev.* 2014, **114**, 11751-11787.
2 Q. Pang, X. Liang, C. Y. Kwok and L. F. Nazar, *Nat. Energy* 2016, **1**, 16132.
3 X. F. Yang, X. Li, K. Adair, H. M. Zhang and X. L. Sun, *Electrochem. Energy Rev.* 2018, **1**, 239-293.
4 Z. Li, H. B. Wu and X. W. Lou, *Energy Environ. Sci.* 2016, **9**, 3061-3070.
5 F. Pei, L. L. Lin, D. H. Ou, Z. M. Zheng, S. G. Mo, X. L. Fang and N. F. Zheng, *Nat. Commun.* 2017, **8**, 482.
6 Y. J. Li, K. K. Fu, C. J. Chen, W. Luo, T. T. Gao, S. M. Xu, J. Q. Dai, G. Pastel, Y. B. Wang, B. Y. Liu, J. W. Song, Y. N. Chen, C. P. Yang and L. B. Hu, *ACS Nano* 2017, **11**, 4801−4807.
7 W. Chen, T. Qian, J. Xiong, N. Xu, X. J. Liu, J. Liu, J. Q. Zhou, X. W. Shen, T. Z. Yang, Y. Chen and C. L. Yan, *Adv. Mater.* 2017, **29**, 1605160.
8 H. Yuan, J. Q. Huang, H. J. Peng, M. Titirici, R. Xiang, R. J. Chen, Q. B. Liu and Q. Zhang, *Adv. Energy Mater.* 2018, **8**, 1802107.
9 S. Y. Bai, X. Z. Liu, K. Zhu, S. C. Wu and H. S. Zhou, *Nat. Energy* 2016, **1**, 16094.
10 F. Pei, L. L. Lin, A. Fu, S. G. Mo, D. H. Ou, X. L. Fang and N. F. Zheng, *Joule* 2018, **2**, 323-336.
11 H. J. Peng, W. T. Xu, L. Zhu, D. W. Wang, J. Q. Huang, X. B. Cheng, Z. Yuan, F. Wei and Q. Zhang, *Adv. Funct. Mater.* 2016, **26**, 6351-6358.
12 X. B. Cheng, R. Zhang, C. Z. Zhao and Q. Zhang, *Chem. Rev.* 2017, **117**, 10403-10473.
13 D. C. Lin, Y. Y. Liu and Y. Cui, *Nat. Nanotech.* 2017, **12**, 194-206.
14 R. Xu, X. B. Cheng, C. Yan, X. Q. Zhang, Y. Xiao, C. Z. Zhao, J. Q. Huang and Q. Zhang, *Matter* 2019, **1**, 317-344.
15 J. Lopez, A. Pei, J. Y. Oh, G. N. Wang, Y. Cui and Z. N. Bao, *J. Am. Chem. Soc.* 2018, **140**, 11735-11744.
16 F. Pei, A. Fu, W. B. Ye, J. Peng, X. L. Fang, M. S. Wang and N. F. Zheng, *ACS Nano* 2019, **13**, 8337-8346.
17 Z. Lin, T. F. Liu, X. P. Ai and C. D. Liang, *Nat. Commun.* 2018, *9*, 5262.
18 A. Bhargav, J. R. He and A. Gupta, *Joule* 2020, **4**, 285-291.
19 S. H. Chung, C. H. Chang and A. Manthiram, *Adv. Funct. Mater* 2018, **28**, 1801188.
20 J. Z. Chen, W. A. Henderson, H. L. Pan, B. R. Perdue, R. G. Cao, J. Z. Hu, C. Wan, K. S. Han, K. T. Mueller, J. G. Zhang, Y. Y. Shao and J. Liu, *Nano Lett* 2017, **17**, 3061-3067.
21 Q. Zhao, J. X. Zheng and L. Archer, *ACS Energy Letters* 2018, *3*, 2104-2113.
22 Y. L. Cao, M. Li, J. Lu, J. Liu and K. Amine, *Nat. Nanotech.* 2019, **14**, 200-207.
23 M. Zhao, B. Q. Li, H. J. Peng, H. Yuan, J. Y. Wei and J. Q. Huang, *Angew. Chem. Int. Ed.*, 2020, **59**, 12636–12652.
24 J Liu, Z. N. Bao, Y. Cui, E. J. Dufek, J. B. Goodenough, P. Khalifah, Q. Y. Li, B. Y. Liaw, P. Liu, A. Manthiram, Y. S. Meng, V. R. Subramanian, M. F. Toney, V. V. Viswanathan, M. S. Whittingham, J. Xiao, W. Xu, J. H. Yang, X. Q. Yang and J. G. Zhang, *Nat. Energy* 2019, **4**, 180-186.
25 Q. Pang, A. Shyamsunder, B. Narayanan, C. Y. Kwok, L. A. Curtiss and L. F. Nazar, *Nat. Energy* 2018, **3**, 783-791.
26 Y. X. Yang, Y. R. Zhong, Q. W. Shi, Z. H. Wang, K. N. Sun and H. L. Wang, *Angew. Chem. Int. Ed.* 2018, **57**, 15549-15552.
27 H. L. Pan, K. S. Han, M. H. Engelhard, R. G. Cao, J. Z. Chen, J. G. Zhang, K. T. Mueller, Y. Y. Shao and J. Liu, *Adv. Funct. Mater.* 2018, **28**, 1707234.
28 M. Li, Y. N. Zhang, Z. Y. Bai, W. W. Liu, T. C. Liu, J. Gim, G. P. Jiang, Y. F. Yuan, D. Luo, K. Feng, R. S. Yassar, X. L. Wang, Z. W. Chen and J. Lu, *Adv. Mater.* 2018, **30**, 1804271.
29 W. J. Xue, Z. Shi, L. M. Suo, C. Wang, Z. Q. Wang, H. Z. Wang, K. P. So, A. Maurano, D. W. Yu, Y. M. Chen, L. Qie, Z. Zhu, G. Y. Xu, J. Kong and J. Li, *Nat. Energy* 2019, **4**, 374-382.
30 R. S. Chen, Q. H. Li, X. Q. Yu, L. Q. Chen and H. Li, *Chem. Rev.*, 2020, **120**, 6820-6877.
31 M. Yan, W. P. Wang, Y. X. Yin, L. J. Wan and Y. G. Guo, *EnergyChem* 2019, **1**, 100002.
32 D. N. Lei, K. Shi, H. Ye, Z. P. Wan, Y. Y. Wang, L. Shen, B. H. Li, Q. H. Yang, F. Y. Kang and Y. B. He, *Adv. Funct. Mater.* 2018, **28**, 1707570.
33 K. Fu, Y. H. Gong, G. T. Hitz, D. W. Mcowen, Y. J. Li, S. M. Xu, Y. Wen, L. Zhang, C. W. Wang, G. Pastel, J. Q. Dai, B. Y. Liu, H.

Xie, Y. G. Yao, E. D. Wachsman and L. B. Hu, *Energy Environ. Sci.* 2017, **10**, 1568-1575.
34 I. Osada, H. D. Vries, B. Scrosati and S. Passerini, *Angew. Chem. Int. Ed.* 2016, **55**, 500-513.
35 Z. Y. Lin, X. W. Guo and H. J. Yu, *Nano Energy* 2017, **41**, 646-653.
36 H. P. Wu, Y. Cao, H. P. Su and C. Wang, *Angew. Chem. Int. Ed.* 2018, **57**, 1361-1365.
37 G. H. Chen, F. Zhang, Z. M. Zhou, J. R. Li and Y. B. Tang, *Adv. Energy Mater.* 2018, **8**, 1801219.
38 M. Liu, D. Zhou, Y. B. He, Y. Z. Fu, X. Y. Qin, C. Miao, H. D. Du, B. H. Li, Q. H. Yang, Z. Q. Lin, T. S. Zhao and F. Y. Kang, *Nano Energy* 2016, **22**, 278-289.
39 T. Chen, W. H. Kong, Z. W. Zhang, L. Wang, Y. Hu, G. Y. Zhu, R. P. Chen, L. B. Ma, W. Yan, Y. R. Wang, J. Liu and Z Jin, *Nano Energy* 2018, **54**, 17-25.
40 J. Q. Zhou, H. Q. Ji, J. Liu, T. Qian and C. L. Yan, *Energy Storage Mater.* 2019, **22**, 256-264.
41 D. Zhou, D. Shanmukaraj, A. Tkacheva, M. Armand and G. X. Wang, *Chem*, 2019, **5**, 2326-2352.
42 J. Cao, L. Wang, Y. M. Shang, M. Fang, L. F. Deng, J. Gao, J. J. Li, H. Chen and X. M. He, *Electrochimica Acta* 2013, **111**, 674-679.
43 W. L. Li, Y. J. Xing, X. Y. Xing, Y. H. Li, G. Yang and L. X. Xu, *Electrochimica Acta* 2013, **112**, 183-190.
44 H. J. Huang, F. Ding, H. Zhong, H. Li, W. G. Zhang, X. G. Liu and Qiang Xu, *J. Mater. Chem. A*, 2018, 6, 9539-9549.
45 S. T. Zheng and G. Y. Yang, *Chem. Soc. Rev.* 2012, **41**, 7623-7646.
46 X. Y. Zheng, J. Xie, X. J. Kong, L. S. Long and L. S. Zheng, *Coord. Chem. Rev.* 2019, **378**, 222-236.
47 W. H. Fang, L. Zhang and J. Zhang, *Chem. Soc. Rev.* 2018, **47**, 404-421.
48 S. J. Wang, H. Reinsch, N. Heymans, M. Wahiduzzaman, C. Martineaucorcos, G. D. Weireld, G. Maurin and C. Serre, *Matter* 2020, **2**, 440-450.
49 S. Choudhury, R. Mangal, A. Agrawal and L. A. Archer, *Nat. Commun.* 2015, **6**, 10101.
50 D. C. Lin, W. Liu, Y. Y. Liu, H. R. Lee, P. C. Hsu, K. Liu and Y. Cui, *Nano Lett.*, 2016, **16**, 459–465.
51 C. W. Zhao, Y. Z. Han, S. Q. Dai, X. M. Chen, J. Z. Yan, W. J. Zhang, H. F. Su, S. C. Lin, Z. C. Tang, B. K. Teo and N. F. Zheng, *Angew. Chem. Int. Ed.* 2017, **56**, 16252-16256.
52 W. D. Li, E. M. Erickson and A. Manthiram, *Nat. Energy* 2020, **5**, 26-34.
53 C. C Fang, J. X. Li, M. H. Zhang, Y. H. Zhang, F. Yang, J. Z. Lee, M. H. Lee, J. Alvarado, M. A. Schroeder, Y. C. Y. Yang, B. Y. Lu, N. Williams, M. Ceja, L. Yang, M. Cai, J. Gu, K. Xu, X. F. Wang and Y. S. Meng, *Nature* 2019, **572**, 511.
54 G. M. Zhou, F. Li and H. M. Cheng, *Energy Environ. Sci.* 2014, **7**, 1307.
55 J. Chang, J. Shang, Y. M. Sun, L. K. Ono, D. R. Wang, Z. J. Ma, Q. Y. Huang, D. D. Chen, G. Q. Liu, Y. Cui, Y. B. Qi and Z. J. Zheng, *Nat. Commun.* 2018, **9**, 4480.
56 M. S. Balogun, H. Yang, Y. Luo, W. T. Qiu, Y. C. Huang, Z. Q. Liu and Y. X. Tong, *Energy Environ. Sci.,* 2018, **11**, 1859-1869.
57 Y. C. Huang, H. Yang, T. Z. Xiong, D. Adekoya, W. T. Qiu, Z. M. Wang, S. Q. Zhang and M. S. Balogun, *Energy Storage Mater.*, 2020, **25**, 41–51.
58 T. Xiong, H. Su, F. Yang, Q. Tan, P. B. S. Appadurai , A. A. Afuwape, K. Guo, Y. Huang, Z. Wang and M. S. Balogun, *Mater. Today Energy,* 2020, **17**, 100461.

TOC

Titanium-oxo clusters reinforced gel polymer electrolyte is developed to improve the performance of high-sulfur-loading lithium-sulfur batteries under lean electrolyte conditions.